Structure and chemical bonding of UAuGe

2001 J. Phys.: Condens. Matter 13 3123

(http://iopscience.iop.org/0953-8984/13/13/321)

INSTITUTE OF PHYSICS PUBLISHING JOURNAL OF PHYSICS: CONDENSED MATTER

J. Phys.: Condens. Matter **13** (2001) 3123–3137 www.iop.org/Journals/cm PII: S0953-8984(01)21515-X

Structure and chemical bonding of UAuGe

B J Gibson[1], R K Kremer[1], O Jepsen[1], J D Garrett[2], R-D Hoffmann[3] and R Pöttgen[3]

[1] Max-Planck-Institut für Festkörperforschung, Heisenbergstraße 1, D-70569 Stuttgart, Germany
[2] Brockhouse Institute for Materials Research, McMaster University, Hamilton, Ontario, Canada, L8S 4M1
[3] Department Chemie, Ludwig-Maximilians-Universität, Butenandtstraße 5-13 (Haus D), D-81377 München, Germany

Received 30 January 2001

Abstract

UAuGe was prepared from the elements by reaction in an arc-melting furnace and subsequent annealing at about 1200 K in a water-cooled silica tube in a high-frequency furnace. UAuGe crystallizes from the melt and is also stable at 920 K. It has the hexagonal YPtAs-type structure: $P6_3/mmc$, with $a = 435.26(4)$ pm, $c = 1547.4(1)$ pm, $V = 0.2539(1)$ nm^3, $wR2 = 0.0785$, 144 F^2-values, and 12 variables. The structure of UAuGe may be considered as a superstructure with a quadrupled c-axis of the well known AlB_2 type. The gold and germanium atoms order on the boron positions and form two-dimensionally infinite puckered layers of Au_3Ge_3 hexagons with intralayer Au–Ge distances of 257 pm. Between adjacent layers the gold atoms have weak secondary Au–Au interactions with Au–Au distances of 327 pm. *Ab initio* calculations of the electronic band structure using the tight-binding linear muffin-tin orbital method are presented. The bonding is illustrated by valence charge density and crystal orbital Hamiltonian population plots which are compared with those of ScAuSi which has a similar structure with Au–Au interactions between the layers. The Au–Au bonding is however much weaker in UAuGe than in ScAuSi. Resistivity measurements exhibit a non-metallic temperature dependence. The increase in resistivity towards lower temperatures is uncharacteristic of intermetallic compounds, and may be fitted to a Curie–Weiss-type formula, suggesting a direct correlation to the magnetic ordering. A maximum in the resistivity is observed at $T = 26(1)$ K.

1. Introduction

The series of equiatomic rare-earth–gold germanides [1–8] has been intensively investigated in recent years because of their greatly varying magnetic and electrical properties. Except for the europium compound EuAuGe with its own type of structure [2, 5], all rare-earth-containing (Ln-containing) germanides LnAuGe derive from an ordered $CaIn_2$-type [9] structure, a superstructure of the AlB_2 type [10]. Ordering of gold and germanium atoms on the indium positions leads to the NdPtSb-type [11] or the LiGaGe structure with the same space group [12, 13]. The gold and germanium atoms form puckered Au_3Ge_3 hexagons with

strong Au–Ge intralayer interactions. Depending on the size of the respective rare-earth atom, flat layers without interlayer Au–Ge interactions can be observed (structure of the CeAuGe, NdPtSb type), or significant Au–Ge interlayer bonding occurs, as in the structure of the ScAuGe (LiGaGe) type with Sc being the smallest rare-earth atom [4]. This peculiar situation regarding the chemical bonding was investigated in greater detail in reference [4].

An equiatomic germanide is also known, with uranium as the electropositive component [14]. Tran and Troć proposed [14] isotypism with the orthorhombic $CeCu_2$-type [15] or TiNiSi-type [16] structure on the basis of x-ray powder data and they determined some preliminary magnetic data. Details of the UAuGe structure, however, were not studied. In the course of our systematic studies on the equiatomic gold germanides, we have reinvestigated the crystal structure of UAuGe in order to determine the ordering between the gold and germanium atoms within the polyanionic network. These investigations unambiguously revealed that UAuGe crystallizes with the YPtAs-type structure [11], a superstructure of the AlB_2 type. The superstructure reflections have most probably been overlooked in previous work. The crystal chemistry, chemical bonding, and first electrical transport properties of UAuGe are reported herein. A detailed study of the magnetic properties of UAuGe will be presented in a forthcoming publication.

2. Experimental procedure

The starting materials for the preparation of the UAuGe were ingots of uranium, gold wire, and germanium lumps, all with stated purities better than 99.9%. The elemental components were mixed in the ideal 1:1:1 atomic ratio and melted to buttons in an arc furnace under an argon pressure of about 800 mbar. The argon was purified over molecular sieves and a titanium sponge (900 K). The melted ingot was turned over and remelted three times on each side to ensure homogeneity. The arc-melted UAuGe button was cut into several pieces. One fragment was enclosed in an evacuated silica tube and put in a water-cooled sample chamber of a high-frequency furnace. The piece was first melted again and subsequently annealed at about 1200 K for about four hours to increase crystallinity. The resulting silvery product was extremely brittle and well crystallized. Another fragment was first remelted, but then quenched, and two further pieces were annealed in evacuated silica tubes for 11 days at 920 K and 1070 K; this was followed by rapid cooling to room temperature. Polycrystalline UAuGe is stable in moist air over a period of several weeks. No deterioration could be observed. The powders are light grey. The platelet-shaped single crystals exhibit metallic lustre.

The purity of the samples was checked by obtaining Guinier powder patterns using Cu Kα_1 radiation and α-quartz ($a = 491.30$ pm, $c = 540.46$ pm) as an internal standard. The lattice constants (table 1) were obtained by least-squares refinements of the powder data. The indexing of the diffraction lines was facilitated by intensity calculations [17] using the positional parameters of the refined structure. To compare the calculated intensities with the experimental values more accurately, the Guinier photographs of the four samples were scanned with a microdensitometer (Line Scanner LS-20/KEJ Instruments) and analysed using programs supplied by the manufacturer. Profile analyses were carried out using commercial fitting routines. The complete list of the powder data is given in table 2.

Single-crystal intensity data were collected at room temperature using a four-circle diffractometer (Enraf-Nonius CAD4) using graphite-monochromatized Mo Kα radiation ($\lambda = 71.073$ pm) and a scintillation counter with pulse height discrimination. An empirical absorption correction was applied on the basis of ψ-scan data. All relevant parameters concerning the data collection are listed in table 1.

Table 1. Crystal data and structure refinement for UAuGe.

Empirical formula	UAuGe
Molar mass	507.59 g mol^{-1}
Pearson symbol	hP12
Crystal system	Hexagonal
Space group	$P6_3/mmc$ (No 194)
Unit-cell dimensions	$a = 435.26(4)$ pm
(Guinier powder data)	$c = 1547.4(1)$ pm
	$V = 0.2539(1)$ nm^3
Formula units per cell	$Z = 4$
Calculated density	13.28 g cm^{-3}
Crystal size	$45 \times 35 \times 25$ μm^3
Transmission ratio (max/min)	2.84
Absorption coefficient	132.6 mm^{-1}
$F(000)$	812
θ-range for data collection	2° to 28°
Scan type	$\omega/2\theta$
Range in hkl	±5, ±5, ±20
Total No of reflections	2132
Independent reflections	144 ($R_{\rm int} = 0.1253$)
Reflections with $I > 2\sigma(I)$	124 ($R_{\rm sigma} = 0.0402$)
Data/restraints/parameters	144/0/12
Goodness of fit to F^2	1.296
Final R-indices ($I > 2\sigma(I)$)	$R1 = 0.0301$, $wR2 = 0.0691$
R-indices (all data)	$R1 = 0.0366$, $wR2 = 0.0785$
Extinction coefficient	0.0010(3)
Largest diffraction peak and hole	4139 and -5704 e nm^{-3}

The electronic structures of UAuGe and ScAuSi were calculated *ab initio* using the self-consistent TB-LMTO-ASA method [18]. A non-local exchange–correlation potential was used [19] and all relativistic effects were included except for the spin–orbit coupling. The LMTO method has been described fully elsewhere [18, 20] and we shall therefore only give some technical data for the calculations in table 3.

In this table the inclusion of a partial wave (s: angular momentum 0; p: angular momentum 1, and so on) in the LMTO basis set is indicated by an *l* (meaning low) and an included partial wave, which has been down-folded, is indicated by an *i* (meaning intermediate). *S* is the sphere radius in atomic units and E indicates interstitial spheres, which had to be inserted in order for the volume of all spheres in the unit cell to equal the unit-cell volume. No overlap between two atomic centred spheres exceeded 16% and the overlap between an atomic sphere and an interstitial sphere never exceeded 18%. The interstitial spheres were at the $\boldsymbol{a}/3 + 2\boldsymbol{b}/3 + 3\boldsymbol{c}/4$ equivalent positions (Wyckoff 2d) for UAuGe and $\boldsymbol{a}/3 + 2\boldsymbol{b}/3$ (Wyckoff 1c) for ScAuSi. The sphere radii and the positions of the interstitial spheres were determined by an automatic algorithm developed by Krier *et al* [21].

The calculations were very similar to those in references [4] and [6] except for the use of a non-local exchange–correlation potential, and we used 96 and 124 irreducible points in the tetrahedron k-space integration [22] for UAuGe and ScAuSi, respectively.

In order to obtain a magnetic ground state, the calculations for UAuGe were performed with spin unrestricted.

Table 2. Guinier powder data (Cu Kα_1 radiation) for UAuGe. Superstructure reflections are marked with an asterisk (i.e. hkl: $l \neq 4n$). I_o-values were obtained by use of a Guinier film scanner.

h	k	l	$2\theta_o$	d_o (Å)	d_c (Å)	I_c	I_o
0	0	2*	11.41	7.7519	7.7371	2	2
0	0	4	23.00	3.8633	3.8685	< 1	< 1
1	0	0	23.55	3.7743	3.7695	8	12
1	0	1*	24.26	3.6653	3.6624	15	17
1	0	2*	26.28	3.3880	3.3887	< 1	< 1
1	0	3*	29.30	3.0453	3.0434	< 1	< 1
1	0	4	33.15	2.7000	2.6998	100	100
0	0	6*	34.76	2.5786	2.5790	1	< 1
1	0	5*	37.58	2.3914	2.3919	13	14
1	1	0	41.46	2.1762	2.1763	57	62
1	0	6*	42.46	2.1274	2.1285	1	1
1	1	2*	43.16	2.0945	2.0950	1	< 1
0	0	8	46.94	1.9340	1.9343	9	8
1	0	7*	47.63	1.9076	1.9069	2	2
1	1	4	47.92	1.8967	1.8968	< 1	1
2	0	0	48.23	1.8853	1.8847	1	2
2	0	1*	48.61	1.8714	1.8709	3	2
1	0	8	53.16	1.7214	1.7209	5	7
2	0	4	54.07	1.6946	1.6943	29	41
1	1	6*	55.17	1.6634	1.6633	2	1
2	0	5*	57.18	1.6097	1.6097	4	4
1	0	9*	58.99	1.5644	1.5643	5	3
1	1	8	64.37	1.4460	1.4458	24	27
2	0	7*	64.97	1.4342	1.4342	1	4
2	1	0*	65.46	1.4246	1.4247	1	2
2	1	1*	65.77	1.4186	1.4187	3	2
2	0	8	69.59	1.3498	1.3499	3	3
2	1	4	70.35	1.3371	1.3369	33	42
1	0	11*	71.53	1.3180	1.3180	3	1
2	1	5*	73.04	1.2943	1.2942	5	3
2	0	9*	74.67	1.2701	1.2702	3	1
3	0	0	75.64	1.2562	1.2565	15	9
1	0	12	78.30	1.2200	1.2201	< 1	< 1
2	1	7*	80.53	1.1976	1.1976	1	< 1

Table 3. Technical data concerning the band-structure calculations for UAuGe and ScAuSi (see the text for details).

	s	p	d	f	S (au)		s	p	d	f	S (au)
U1	*l*	*l*	*l*	*l*	3.867	Sc1	*l*	*i*	*l*		3.461
U2	*l*	*l*	*l*	*l*	3.747	Sc2	*l*	*i*	*l*		3.326
Au	*l*	*l*	*l*	*i*	2.827	Au	*l*	*l*	*l*	*i*	2.762
Ge	*l*	*l*	*i*		2.791	Si	*l*	*l*	*i*		2.701
E	*l*	*i*	*i*		1.757	E	*l*	*i*	*i*		1.726

Resistivity measurements were performed on a small bar ($\approx 2.3 \times 1.0 \times 0.5$ mm^3), cut with a diamond saw from a polycrystalline ingot. A conventional d.c. four-probe set-up was utilized allowing measurements between 2 K and 300 K. The cooling and heating curves taken at a constant current were identical within error limits.

3. Results and discussion

3.1. Lattice parameters

In a previous investigation, Tran and Troć assigned the orthorhombic $CeCu_2$-type (space group $Imma$) or TiNiSi-type (space group $Pnma$, a ternary-ordered variant of $CeCu_2$) structure to UAuGe and they obtained by refinement the lattice parameters $a = 436.7$ pm, $b = 763.8$ pm, $c = 752.3$ pm, and $V = 0.2509$ nm^3. Our highly resolved Guinier powder diagrams, however, did not match with this orthorhombic unit cell. The intensity distribution for a calculated TiNiSi-type arrangement [17] did not match with our experimental patterns either. The assumption of an orthorhombic structure is thus highly questionable. Instead, we were able to index the powder pattern hexagonally (table 2), in agreement with our single-crystal film data discussed below, on the basis of an AlB_2-related cell with a quadrupled c-axis with the lattice parameters $a = 435.26(4)$ pm, $c = 1547.4(1)$ pm, and $V = 0.25388(4)$ nm^3. The strongest reflections were compatible with the pronounced AlB_2-type subcell with lattice parameter $c/4$. The previously reported data for the orthorhombic cell and those for the hexagonal cell have the following approximate relations: $a_o \approx a_h$; $b_o \approx (1/2)c_h$, and $c_o \approx a_h\sqrt{3}$. The many superstructure reflections have most probably been overlooked in the previous investigation. In particular the *101* and the *105* reflections were unmistakably observed. Their experimentally integrated intensities of 17% and 14% matched the calculated relative intensities of 15% and 13%, respectively. The lattice constants derived from the quenched and the other two samples (1070 K and 920 K) agreed well with those for the 1200 K sample; their lattice constants were: $a = 435.5(2)$ pm, $c = 1543.9(6)$ pm, $V = 0.2536$ nm^3 for the quenched sample; $a = 435.38(8)$ pm, $c = 1545.4(2)$ pm, $V = 0.2537$ nm^3 for the 920 K sample; and $a = 435.48(8)$ pm, $c = 1544.4(2)$ pm, $V = 0.2537$ nm^3 for the 1070 K sample. No phase transition was observed, in contrast to what might have been expected considering the data reported by Tran and Troć. Differences arose, of course, due to the differing crystallinity of the four samples. Therefore, profile analyses for two reflections were carried out. The full widths at half-maximum (fwhm) of the *100* and *101* reflections at $2\theta = 23.56^\circ$ and 24.26° were determined using a Lorentzian function neglecting instrumental broadening. The fwhm (in units of 2θ degrees) were as follows for the *100* (*101*) reflection: 0.17 (0.16), 0.08 (0.09), 0.10 (0.10), and 0.11 (0.12) for the quenched, 1200 K, 1070 K, and 920 K samples, respectively. It is understandable that the quenched sample as compared to the annealed samples has the lowest crystallinity with reflections twice as broad. Clearly, the higher temperature allows faster atomic diffusion and, thus, better crystallinity.

3.2. Structure refinement

Single crystals of UAuGe were isolated from the crushed samples and examined by Buerger precession photographs to establish both the symmetry and the suitability for intensity data collection. The different crystallinities of the various samples were also noticeable in the Laue photographs. Crystals of the quenched sample showed rather elongated diffraction spots, while crystals taken from the 1200 K sample showed an almost circular shape. Two crystals were investigated further. Their photographs (reciprocal layers hhl, $h0l$, and $h1l$) showed a pronounced AlB_2-like hexagonal subcell with Laue symmetry $6/mmm$ and weak superstructure reflections which force a quadrupling of the c-axis. The systematic extinctions (hhl only observed with $l = 2n$) led to the possible space groups $P6_3/mmc$ and $P6_3mc$. The structure refinement eventually showed that the space group with the highest symmetry compatible with these extinctions, $P6_3/mmc$, was the correct one. All relevant crystallographic data and experimental details are listed in table 1.

In the course of our systematic investigations on AlB_2-related superstructures [23], we readily recognized that the UAuGe structure might be isotypic with the YPtAs structure [11]. Thus, the atomic positions of YPtAs were taken as starting parameters and the structure was successfully refined using SHELXL-97 (full-matrix least-squares fitting to F^2) [24] with anisotropic displacement parameters for all atoms.

A final difference Fourier synthesis was flat except for residual peaks at the gold position. This can be accounted for by a probably incomplete absorption correction. A second single crystal with smaller dimensions ($10 \times 20 \times 25\ \mu m^3$) showed the same tendencies. The results of the two single-crystal refinements were identical within the error limits. The residual peaks for the smaller crystal were lower, but because of the small size, the weak superstructure reflections, in particular, did not have the same high quality as those of the larger crystal, and the standard deviations came out about twice as large. Therefore, the results for the larger crystal are reported herein (table 1), even though the data are hampered by absorption. Atomic coordinates and interatomic distances are listed in tables 4 and 5. The refinement converged to low residuals. These R-values, however, are strongly affected by the stronger subcell reflections. We therefore prefer to calculate separate residuals for the superstructure reflections in order to evaluate the quality of the structure refinement. For all 144 reflections we obtained low residuals of $R1 = 0.0534$ for 99 superstructure reflections [25] and of $R1 = 0.0251$ for 45 subcell reflections. Listings of the anisotropic displacement parameters and the observed and calculated structure factors are available[1].

Table 4. Atomic coordinates and isotropic displacement parameters (pm^2) for UAuGe. U_{eq} is defined as one third of the trace of the orthogonalized U_{ij}-tensor.

Atom	Wyckoff site	x	y	z	U_{eq} (pm^2)
U1	2a	0	0	0	42(5)
U2	2b	0	0	1/4	62(5)
Au	4f	1/3	2/3	0.14441(9)	103(5)
Ge	4f	1/3	2/3	0.6107(2)	42(8)

Table 5. Interatomic distances (pm) in the structure of UAuGe. All distances shorter than 525 pm (U–U, U–Au, U–Ge), 420 pm (Au–Au, Ge–Ge), and 390 pm (Au–Ge) are listed. The standard deviations are all equal to or less than 0.5 pm.

U1:	6	Ge	304.1	Au:	3	Ge	256.7
	6	Au	336.3		3	U2	299.7
	2	U2	386.9		1	Au	326.8
	6	U1	435.3		3	U1	336.3
U2:	6	Au	299.7	Ge:	3	Au	256.7
	6	Ge	331.1		3	U1	304.1
	2	U1	386.9		3	U2	331.1
	6	U2	435.3				

3.3. Crystal chemistry

The structure of UAuGe has been determined from single-crystal x-ray diffractometer data. It is clear now that UAuGe adopts the YPtAs-type structure [11], a superstructure of the AlB_2

[1] The details may be obtained from: Fachinformationszentrum Karlsruhe, D-76344 Eggenstein-Leopoldshafen, Germany, by quoting the registry number CSD-391079.

type [10], and crystallizes with this structure type at least down to 920 K. This structure type has so far only been observed for YPtAs [11], the alkaline-earth compounds CaGaGe, CaGaSn, SrGaGe, SrGaSn, and BaGaGe [26] and UAuGe, as reported herein. Although an orthorhombic cell has been reported in reference [14], we assume that in this previous investigation superstructure reflections have been overlooked. Since UAuSi [14, 27] with SrPtSb-type structure and UAuSn [14, 28] with $CaIn_2$-type structure adopt hexagonal superstructures of AlB_2, it seems reasonable that the germanide adopts a similar atomic arrangement.

The structure of UAuGe is presented in figure 1 together with the structures of ScAuSi [29] and CeAuGe [3]. The gold and germanium atoms form puckered Au_3Ge_3 hexagons with intralayer Au–Ge distances of 257 pm, only slightly larger than the sum of the Pauling single-bond radii [30] of 256 pm for gold and germanium, indicating strong covalent Au–Ge bonding. The stacking sequence of the four Au_3Ge_3 layers in UAuGe is ABB′A′, ABB′A′ as outlined in figure 1. The layers A and A′ are inverted with respect to each other. The same holds true for B and B′. The layers A and B are related by the mirror plane extending perpendicular to the *c*-axis. Due to the inversion, weak Au–Au interactions occur between the A and B (A and B′) layers with Au–Au distances of 327 pm, significantly longer than in fcc gold [31], wherein each gold atom has twelve neighbours at 288 pm. The interlayer Au–Au distances of 316 pm in EuAuGe [2] and of 328 pm in Er_2Au_2Sn [32] may also be considered as weak interactions. All of these distances compare well with those in molecular compounds like $[Au(i\text{-}C_3H_7O)_2PS_2]_2$ [33], $i\text{-}C_3H_7NH_2AuC{\equiv}CC_6H_5$ [34], and $Au(III)(DMG)_2Au(I)Cl_2$ [35], where such secondary Au–Au bonds (291 pm up to 327 pm) are sufficiently strong to cause dimerization in solution and polymerization in the solid state. Similar weak Au–Au interactions were also observed in Au_2P_3 and $Au_7P_{10}I$ [36]. No interlayer interactions are observed between the layers A and A′, and B and B′ (Au–Ge distances of 393 pm).

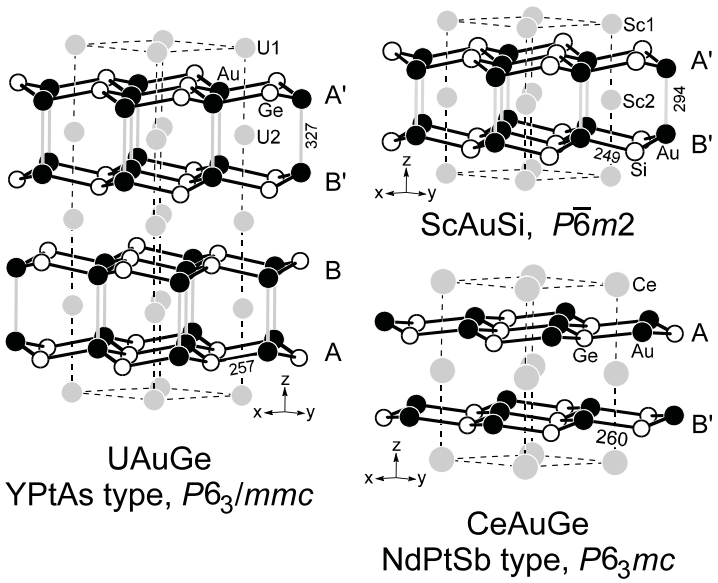

Figure 1. Crystal structures of UAuGe (left), ScAuSi (upper right), and CeAuGe (lower right). The unit cells and the polyanionic networks are outlined. Distances are given in pm. Gold–germanium bonding within the puckered hexagons is indicated by black lines. Grey lines symbolize weak Au–Au bonding between adjacent layers. The various layers are designated by the capital letters A, A′, B, and B′ (see the text for details).

At this point it is worthwhile to compare the structure of UAuGe with the structures of CeAuGe [3] and ScAuSi [29] as emphasized in figure 1. The stacking sequences of the puckered Au_3Ge_3 layers are AB′, AB′ in CeAuGe and A′B′, A′B′ in ScAuSi. In the case of ScAuSi we also observe interlayer Au–Au interactions at the much shorter Au–Au distance of 294 pm. In ScAuGe [4] (with the same point group as CeAuGe), interlayer Au–Ge bonding with Au–Ge distances of 275 pm is observed.

The structure of UAuGe has two crystallographically different uranium sites, both with coordination number (CN) 20. While the U1 atoms have six closer germanium neighbours at 304 pm and six gold neighbours at 336 pm, the U2 atoms have six gold neighbours with smaller U–Au distances of 300 pm and six further germanium neighbours at 331 pm. Additionally, each uranium atom has two uranium neighbours at 387 pm (along the *c*-axis) and six further uranium neighbours at 435 pm (within the *ab*-plane). Both of these distances are well above the Hill limit [37] of about 340 pm for f-electron localization.

UAuGe belongs to a large family of intermetallic compounds derived from the well known AlB_2-type ones. The crystal chemical relationship of AlB_2-related compounds can be arranged in a symmetry tree containing more than 45 structure types [23]. In figure 2, a section of the hexagonal branch is shown following a formalism proposed by Bärnighausen [38,39]. Starting from AlB_2, an isomorphic transition of index 2 leads to the structure of $BaSn_5$ [40], where the tin atoms of the 4h site form two-dimensionally infinite condensed hexagons. These hexagons are formed by the gold and germanium atoms in the structure of UAuGe, and the platinum and arsenic in the prototype YPtAs [11]. In figure 2 the atomic positions of UAuGe are used to show the development of the structural distortions. Ordering gold and germanium atoms in UAuGe again forces doubling of the *c*-axis, which leads to the space group $P6_3/mmc$ via a *klassengleiche* transition of index 2.

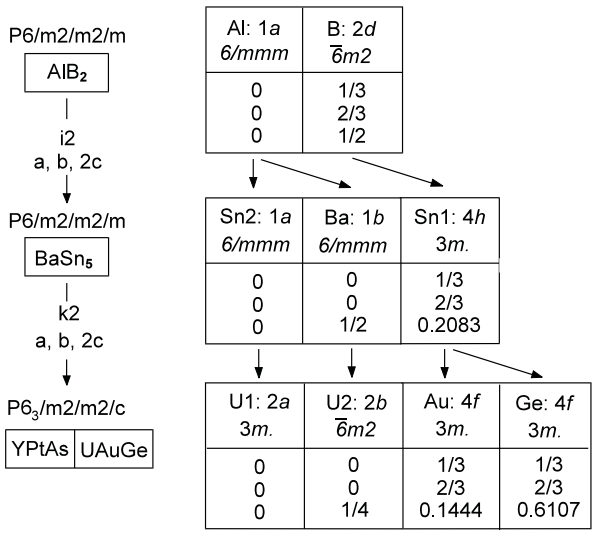

Figure 2. The group–subgroup relationship starting with the aristotype AlB_2 and its derivatives $BaSn_2$, YPtAs, and UAuGe according to the Bärnighausen formalism. The indices of the *klassengleiche* (k) and isomorphic (i) transitions as well as the unit-cell transformations are indicated. On the right-hand side the development of the site symmetries and the variable atomic parameters are given. The ideal *z*-parameters of the 'undistorted' superstructures would be 0.25 for the tin position 4h in the case of $BaSn_5$ and 0.125 (0.625) for the gold (germanium) position of UAuGe.

3.4. Electronic structure

The calculated electronic structures of UAuGe (shown in figure 3) and ScAuSi are very similar to each other and also to our previously calculated structures for gold germanides [4, 6].

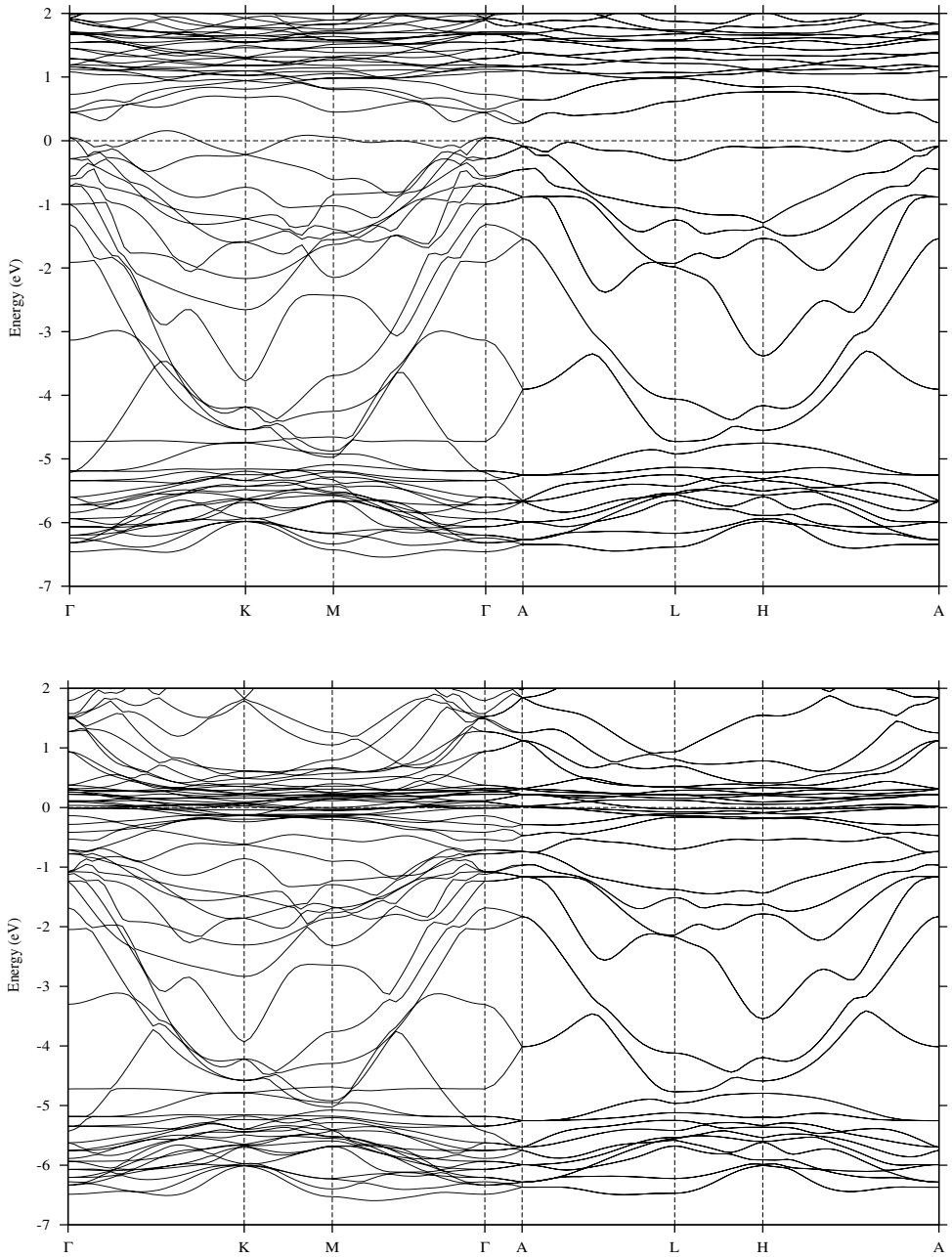

Figure 3. The self-consistent minority-spin energy (upper) and majority-spin energy (lower) band structures of UAuGe along some symmetry lines in the hexagonal Brillouin zone. The zero of energy is at the Fermi level.

The densities of states are shown in figure 4. The Ge/Si s bands are situated around -10 eV (the Fermi level E_F is at 0 eV). The narrow Au d bands are situated around -6 eV. The conduction bands extending from about -5 eV to the Fermi level are the Ge/Si p states. They are nearly filled, and as a consequence a pseudo-gap appears just below the Fermi level in ScAuSi and a real gap in the minority-spin bands of UAuGe appears just above the Fermi level. It should be pointed out that the position of the Fermi level depends sensitively on the strength of the exchange correlation (XC). Increasing the XC moves the Fermi level up in the minority bands. We can therefore not exclude the possibility that on choosing another parametrization of the XC potential the Fermi level will move up to the gap in the minority bands making UAuGe

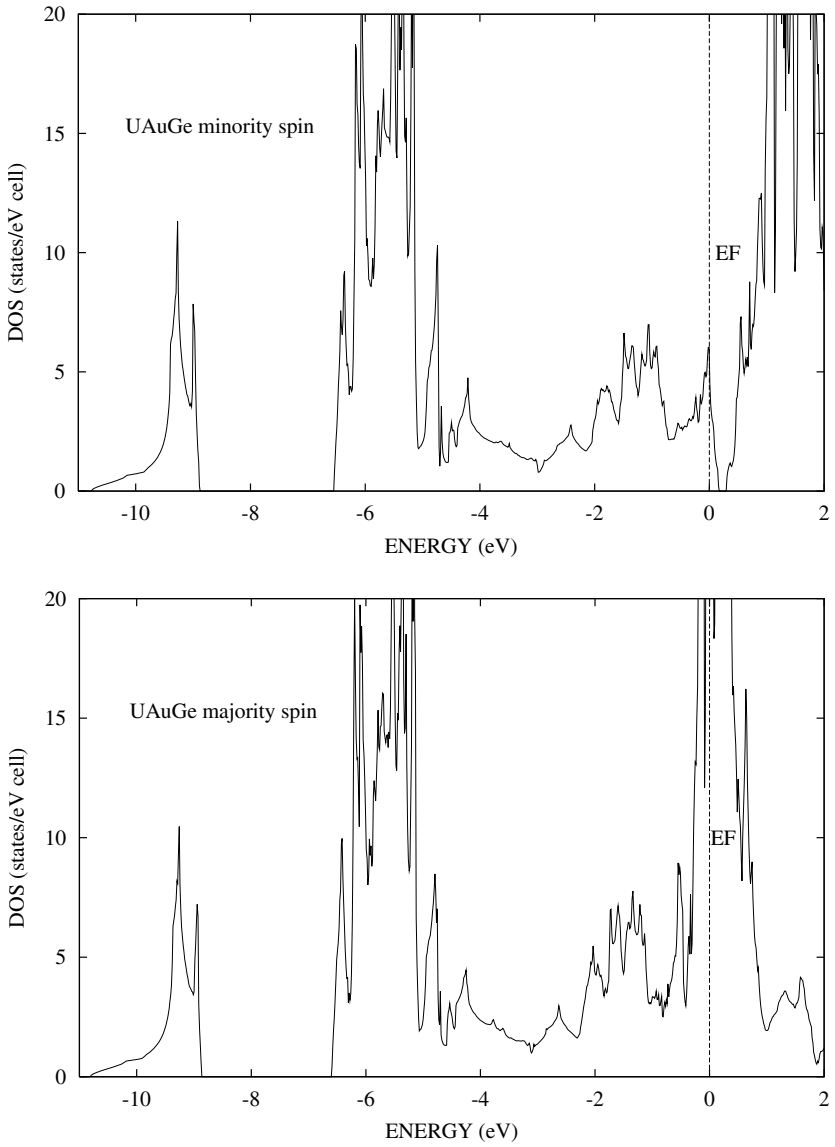

Figure 4. The self-consistent minority-spin (upper) and majority-spin (lower) densities of states of UAuGe. The zero of energy is at the Fermi level.

a so-called half-metallic material [41]. We also performed calculations without the non-local corrections, but the results were similar, i.e. metallic in both spin channels. The main difference between the electronic structures of the two compounds is the appearance of relatively narrow uranium f bands close to the Fermi level. These are unoccupied in the minority-spin channel and partly occupied in the majority-spin channel which results in a relatively large uranium magnetic moment. The presence of magnetism in UAuGe hardly influences the stability of the structure, which for both compounds is achieved by nearly filled Ge/Si p bands due to the donation of three electrons from U/Sc and one electron from Au. The lowest unoccupied bands are formed from U or Sc states.

In figure 5 we show contour plots of the distribution of the total valence charge for UAuGe and ScAuSi. The strong interactions between Au and Ge/Si in the puckered nets are very similar in the two compounds. Perpendicular to the nets, the charge density between the Au in the double layers and between the Si from double layer to double layer is much larger in ScAuSi than in UAuGe.

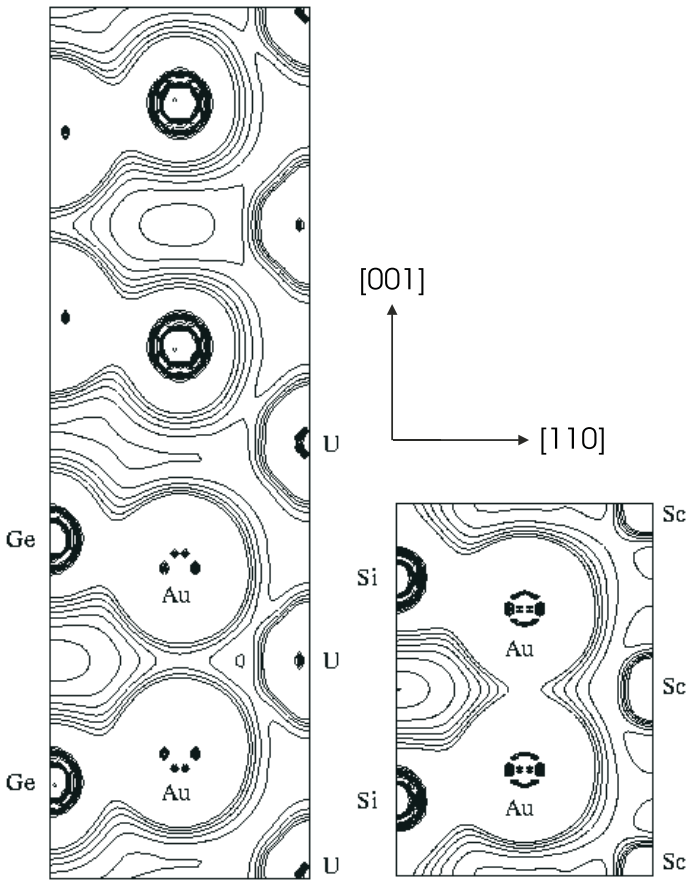

Figure 5. The total valence charge distributions in UAuGe (left) and ScAuSi (right) in the [110]–[001] plane. Eleven contours between 0 and $0.4e/a_0^3$ (a_0 is the Bohr radius) are drawn.

We finally illustrate the bonding in UAuGe and ScAuSi by calculating the Au–Au crystal orbital Hamiltonian population (COHP) [42] between the layers, as shown in figure 6, and the Au–Ge (Au–Si) COHPs in the layer (figure 7). The integrated COHP (ICOHP) at the Fermi

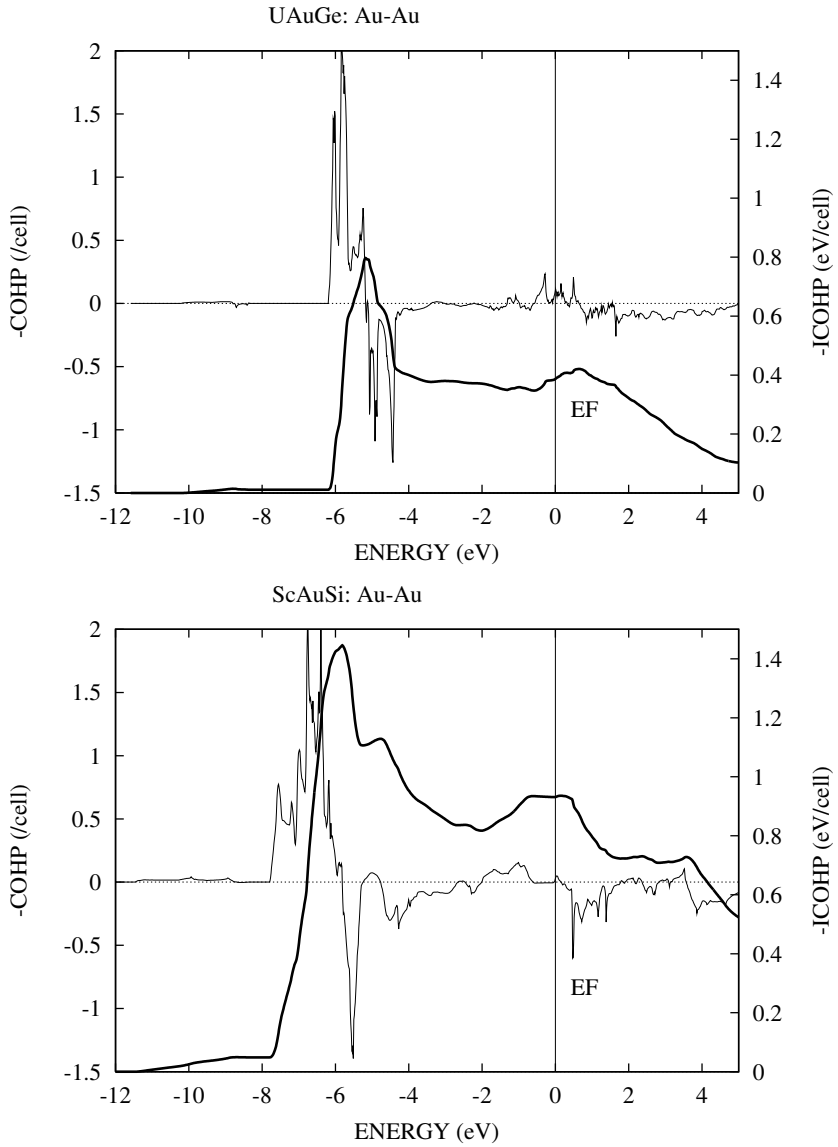

Figure 6. The crystal orbital Hamiltonian population (COHP, thin lines) and integrated COHP (ICOHP, thick lines) for the Au–Au interlayer interactions in UAuGe (upper) and ScAuSi (lower). Note that the signs have been changed so that positive values in the plots correspond to binding.

level is a measure of the strength of the bonding between the two atoms. It may be seen that the Au–Au bonding is considerably larger in ScAuSi than in UAuGe, and that the Au–Si bonding is somewhat larger in ScAuSi than the Au–Ge bonding in UAuGe.

3.5. Electrical resistivity

The electrical resistivity of UAuGe between 2 K and 300 K is shown in figure 8. An increase of the resistivity with decreasing temperature to a maximum at about 26 K is found. This

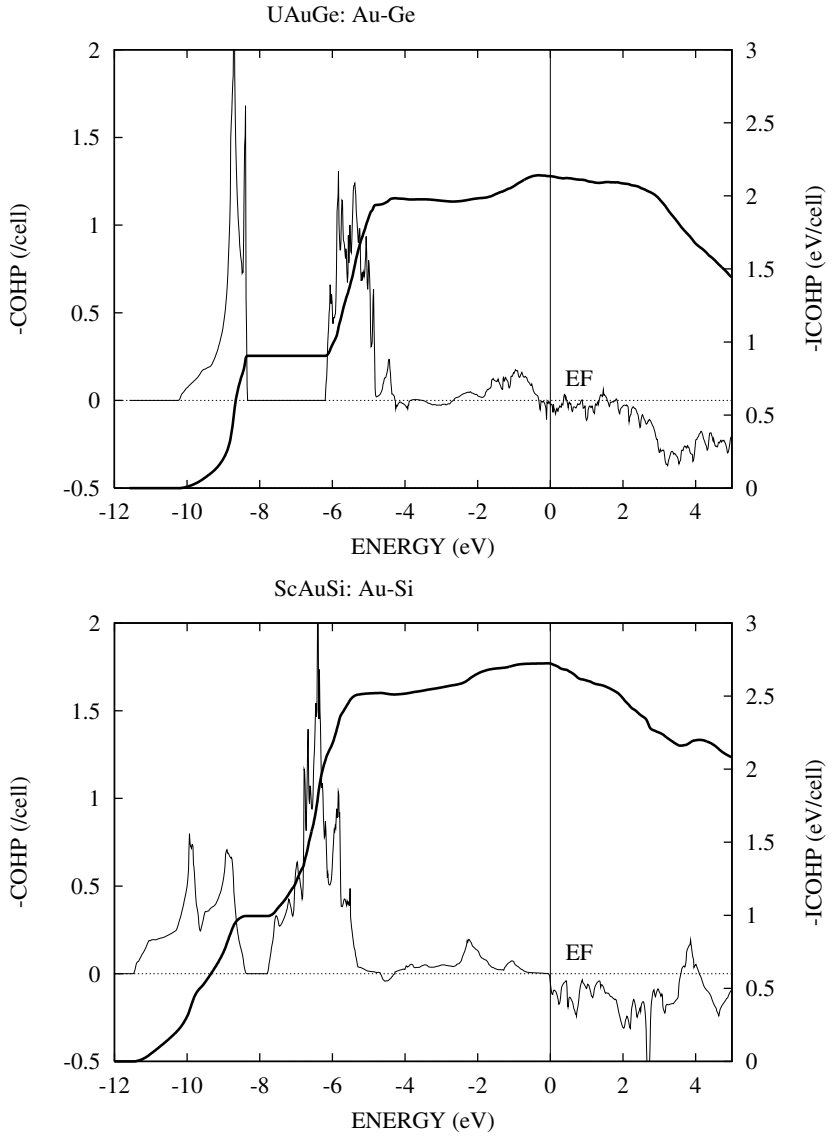

Figure 7. The crystal orbital Hamiltonian population (COHP, thin lines) and integrated COHP (ICOHP, thick lines) for the Au–Ge interlayer interactions in UAuGe (upper) and for the Au–Si interlayer interactions in ScAuSi (lower). Note that the signs have been changed so that positive values in the plots correspond to binding.

'non-metallic' temperature characteristic is to some extent reminiscent of the behaviour of heavy-fermion materials, e.g. $CeAl_3$ [43]. However, the characteristic T^2-dependence of the resistivity found in the prototype heavy-fermion compounds towards lowest temperatures is not observed in UAuGe. A resistivity minimum is also not observed up to room temperature, but we can fit the resistivity above $T_{max} = 26$ K to a Kondo-like logarithmic law with $T^* \approx 40$ K.

However, the resistivity can be equally well fitted by a simple Curie–Weiss-type law, $\rho = A/(T - \Theta) + \rho_0$, with $\Theta = -25(1)$ K (full line in figure 8). Above 100 K this fit is

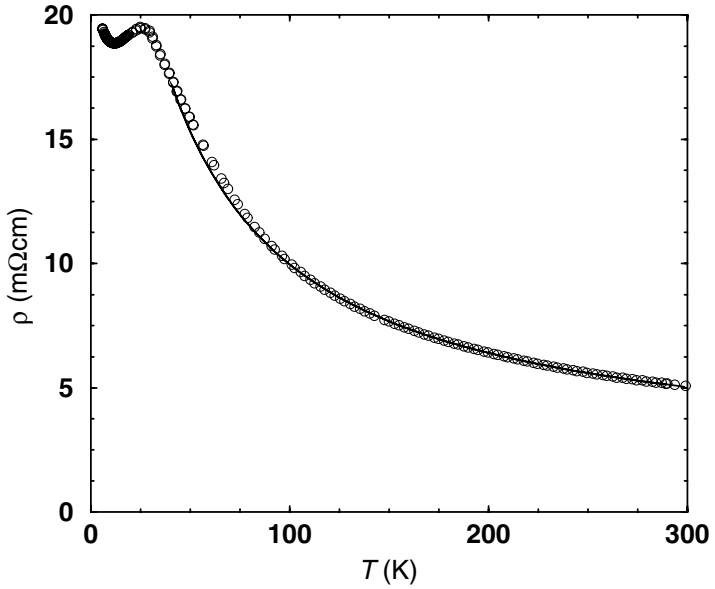

Figure 8. Resistivity of UAuGe. The circles show the measured data. The full line depicts the fit to these data of $\rho = \rho_0 + A/(T - \Theta)$.

good and suggests an intimate correlation between electrical transport and magnetic behaviour. Below $T \approx 80$ K, deviations from the fit occur, corresponding to the anomalies observed in the first susceptibility measurements, $\chi(T)$ [14].

Acknowledgments

We thank Dipl-Ing U Ch Rodewald for the single-crystal data collection and G Siegle for the resistivity measurements. This work was supported by the Deutsche Forschungsgemeinschaft and the Fonds der Chemischen Industrie.

References

[1] Rossi D, Marazza R and Ferro R 1992 *J. Alloys Compounds* **187** 267
[2] Pöttgen R 1995 *J. Mater. Chem.* **5** 505
[3] Pöttgen R, Borrmann H and Kremer R K 1996 *J. Magn. Magn. Mater.* **152** 196
[4] Pöttgen R, Borrmann H, Felser C, Jepsen O, Henn R, Kremer R K and Simon A 1996 *J. Alloys Compounds* **235** 170
[5] Müllmann R, Mosel B D, Eckert H, Pöttgen R and Kremer R K 1997 *Hyperfine Interact.* **108** 389
[6] Schnelle W, Pöttgen R, Kremer R K, Gmelin E and Jepsen O 1997 *J. Phys.: Condens. Matter* **9** 1435
[7] Penc B, Baran S, Ślaski M and Szytula A 1999 *J. Alloys Compounds* **282** L6
[8] Gibson B J, Pöttgen R, Ouladdiaf B, Schnelle W and Kremer R K 2001 *J. Phys.: Condens. Matter* **13** 2593
[9] Iandelli A 1964 *Z. Anorg. Allg. Chem.* **330** 221
[10] Hofmann W and Jäniche W 1935 *Naturwissenschaften* **23** 851
[11] Wenski G and Mewis A 1986 *Z. Kristallogr.* **176** 125
[12] Bockelmann W, Jacobs H and Schuster H-U 1970 *Z. Naturf.* b **25** 1305
[13] Bockelmann W and Schuster H-U 1974 *Z. Anorg. Allg. Chem.* **410** 233
[14] Tran V H and Troć R 1993 *Physica* B **186–188** 744
[15] Larson A C and Cromer D T 1961 *Acta Crystallogr.* **14** 73
[16] Shoemaker C B and Shoemaker D P 1965 *Acta Crystallogr.* **18** 900

[17] Yvon K, Jeitschko W and Parthé E 1977 *J. Appl. Crystallogr.* **10** 73
[18] Andersen O K 1975 *Phys. Rev.* B **12** 3060
Andersen O K and Jepsen O 1984 *Phys. Rev. Lett.* **53** 2571
[19] Perdew J P and Wang Y 1986 *Phys. Rev.* B **33** 8800
[20] Andersen O K, Jepsen O and Glötzel D 1985 *Highlights of Condensed-Matter Theory* ed F Bassani, F Fumi and M P Tosi (New York: North-Holland)
[21] Krier G, Jepsen O and Andersen O K 2001 to be published
[22] Jepsen O and Andersen O K 1971 *Solid State Commun.* **9** 1763
Blöchl P E, Jepsen O and Andersen O K 1994 *Phys. Rev.* B **49** 16 223
[23] Pöttgen R and Hoffmann R-D 2001 *Z. Kristallogr.* **216** 127
[24] Sheldrick G M 1997 *SHELXL-97, Program for Crystal Structure Refinement* University of Göttingen, Germany
[25] Hoffmann R-D 1996 *RWERT—Program for the Calculation of Residuals for Different Classes of Reflections* University of Münster, Germany
[26] Czybulka A, Pinger B and Schuster H-U 1989 *Z. Anorg. Allg. Chem.* **579** 151
[27] Pöttgen R, Tran V H, Hoffmann R-D, Kaczorowski D and Troć R 1996 *J. Mater. Chem.* **6** 429
[28] Palstra T T M, Nieuwenhuys G J, Vlasutin R F M, van der Berg J, Mydosh J A and Buschow K H J 1987 *J. Magn. Magn. Mater.* **67** 331
[29] Fornasini M L, Iandelli A and Pani M 1992 *J. Alloys Compounds* **187** 243
[30] Pauling L 1960 *The Nature of the Chemical Bond and the Structures of Molecules and Crystals* (Ithaca, NY: Cornell University Press)
[31] Donohue J 1974 *The Structures of the Elements* (New York: Wiley)
[32] Pöttgen R 1994 *Z. Naturf.* b **49** 1309
[33] Lawton S L, Rohrbaugh W J and Kokotailo G T 1972 *Inorg. Chem.* **11** 2227
[34] Corfield P W R and Shearer H M M 1967 *Acta Crystallogr.* **23** 156
[35] Rundle R E 1954 *J. Am. Chem. Soc.* **76** 3101
[36] Jeitschko W and Möller M H 1979 *Acta Crystallogr.* B **35** 573
[37] Hill H H 1970 *Plutonium and Other Actinides (Nuclear Materials Series vol 17)* ed W N Mines (New York: AIME) p 2
[38] Bärnighausen H 1980 *Commun. Math Chem.* **9** 139
[39] Bärnighausen H and Müller U 1996 *Symmetriebeziehungen zwischen den Raumgruppen als Hilfsmittel zur straffen Darstellung von Strukturzusammenhängen in der Kristallchemie* University of Karlsruhe and University Gh Kassel, Germany
[40] Fässler T F 2000 private communication
[41] Prinz G A 1998 *Science* **282** 1660
[42] Dronskowski R and Blöchl P 1998 *J. Phys. Chem.* **97** 8617
Boucher F, Jepsen O and Andersen O K 2001 in preparation
[43] Andres K, Graebner J E and Ott H R 1975 *Phys. Rev. Lett.* **35** 1979
Ott H R, Marti O and Hulliger F 1984 *Solid State Commun.* **49** 1129